Fermilab

MicroBooNE Electron-Neutrino Cross-Section Results

FERMILAB-CONF-24-1010-V

PROCEEDINGS OF SCIENCE

MicroBooNE Electron-Neutrino Cross-Section Results

Marina Reggiani-Guzzo[a,*] **on behalf of the MicroBooNE Collaboration**

[a] *University of Edinburgh, School of Physics and Astronomy*
Peter Guthrie Tait Road, James Clerk Maxwell Building, EH9 3FD, Edinburgh

E-mail: mguzzo@ed.ac.uk

Measurement of the electron-neutrino cross-section with argon (ν-Ar) is crucial for current and future neutrino experiments. Results from MicroBooNE detector, a liquid argon time projection chamber (LArTPC) based at Fermilab, provide the most extensive and precise determination of these electron-neutrino cross-sections. MicroBooNE is situated on both on-axis and off-axis beams: the Booster Neutrino Beam (BNB) and Neutrinos at the Main Injector (NuMI) beam, respectively. The background for both beams is dominated by showers from neutral pion decay, necessitating an electron-photon separation technique. In this proceeding, we review three recent electron-neutrino cross-section results from MicroBooNE using NuMI and BNB.

42nd International Conference on High Energy Physics (ICHEP2024)
18-24 July 2024
Prague, Czech Republic

*Speaker

PoS(ICHEP2024)142

1. Introduction

Accurate neutrino cross-section measurements are essential for determining many neutrino oscillation parameters, such as the mixing angle, θ_{13}, and the phase of the CP-violation, δ_{cp}. Neutrino beams are created by striking a target with protons, which creates pions and kaons that decay into muon neutrinos (ν_μ) and antineutrinos ($\bar{\nu}_\mu$). Nearly all measured neutrino cross-sections have been of ν_μ or $\bar{\nu}_\mu$. Because ν_μ in beams oscillate (as a function of L/E) the main channel for long baseline experiments such as T2K, MINOS, and DUNE is electron neutrino (ν_e) appearance. Yet until recently, there have been few direct measurements of ν_e cross sections, most of them using targets other than argon (NOvA [1], T2K [2–4], MINERvA [5], Gargamelle [6]), and only ArgoNeuT [7], which had 13 events, used argon. The determination of ν_e cross sections is thus of great interest for the SBN programme and DUNE.

2. MicroBooNE and its Neutrino Beams

MicroBooNE is a 170-ton LArTPC, with 85 tonnes of active mass. It took data between 2015 and 2021. The location of the MicroBooNE detector allows it to benefit detecting neutrinos coming from two distinct neutrino beams at Fermilab: it is on-axis to the BNB and off-axis the NuMI beams. The more off-axis the detector is, the greater fraction of $\nu_e/\bar{\nu}_e$ in comparison to $\nu_\mu/\bar{\nu}_\mu$. As a consequence, NuMI at MicroBooNE contains approx. 5 times more ν_e in comparison to BNB at the detector. The amount of neutrino flux is commonly quantified as the number of protons on target (POT) used to generate the beam.

3. Electron-Photon Separation Techniques

Charged particles crossing a LArTPC can create two main kinds of signatures inside the detector: a track (caused by protons, muons, charged pions, and characterised by a straight line) or a shower (caused by electrons, positrons, photons, and characterised by the formation of a particle cascade). The main background for ν_e and $\bar{\nu}_e$ analysis is the decay of neutral pions into two photons, $\pi^0 \rightarrow 2\gamma$, which can induce showers in the detector via pair production. This section describes the two primary methods to differentiate electron-induced showers from photon-induced showers.

The first one uses calorimetry information. A photon-induced shower is generated from an electron-positron pair production that further decays into two electron-induced showers. Therefore, a photon-induced shower deposits roughly twice as much energy per unit length (dE/dx) in the start of the electromagnetic shower when compared to an electron-induced one: the measured dE/dx for electron-induced showers peaks around 2 MeV/cm, and for photon-induced showers it peaks around 4 MeV/cm. The second method relies on the fact that photon's delayed shower leads to a gap between the interaction vertex and start of the electromagnetic shower. Compared with electrons, photons produce a delayed shower because they must first decay into an electron-positron pair. Due to this time delay, electrons and photons have different profiles of dE/dx, or energy deposition across a track.

4. Electron-Neutrino Cross-Section Results

MicroBooNE electron-neutrino cross-section results were detailed in three papers, two on NuMI [8, 9], and one on BNB [10]. This section describes the main features of each analysis and their results. All results presented in this document use the Pandora pattern-recognition toolkit [11] to perform the particle signal reconstruction.

NuMI Results. Both NuMI results published by MicroBooNE employ neutrinos from the NuMI neutrino beam in is "neutrino mode", and an integrated exposure to 2.4×10^{20} POT for [8] and 2.0×10^{20} POT for [9]. Both analyses reject beam and cosmic ray interactions that could mimic our signal by combining information from the TPC event topology with information from the optical system. First, we use time information to reject non-beam-induced particle interactions, whose flash time lays outside the NuMI beam spill time window. Then, we use spatial information to reject track-like signals and photon-induced showers, as explained in Section 3.

The first NuMI result [8], published in 2021, measured the flux-averaged inclusive charged-current ν_e and $\bar{\nu}_e$ cross section on argon. It was the first ever ν_e and $\bar{\nu}_e$ inclusive measurement in a large-scale LArTPC on the surface, and the first measurement performed by MicroBooNE using neutrinos coming from the off-axis NuMI beam. This paper demonstrates the electron-photon dE/dx separation power of LArTPCs using a fully automated analysis chain. A final 9.1% selection efficiency and a 38.6% $\nu_e + \bar{\nu}_e$ purity is achieved at the end of the selection chain, resulting in 214 selected $\nu_e + \bar{\nu}_e$ candidates in the data. The cross section measurement is performed on an inclusive sample of charge-current ν_e or $\bar{\nu}_e$ interactions with at least one reconstructed electron-like shower in the final state inside the fiducial volume[1], with $\nu_e + \bar{\nu}_e$ energies above 250 MeV and an average neutrino flux energy at MicroBooNE of 905 MeV with this threshold. This analysis is optimised toward high energies and therefore we set this energy threshold to exclude a region where the efficiency begins to rapidly decrease. No further requirements of additional particles in the final state is used in this analysis. Figure 1 illustrates the flux-averaged inclusive ν_e and $\bar{\nu}_e$ charged-current total cross section on argon in comparison to three different neutrino generators. We found the data cross section to be $6.84 \pm 1.15\,(\text{stat}) \pm 2.33\,(\text{sys}) \times 10^{-39}\,\text{cm}^2/\text{nucleon}$, which is in agreement with the predictions from both GENIE generators and NuWro. The largest systematic uncertainties for this measurement are due to the modelling of the detector and flux simulation.

The second NuMI result [9], published in 2022, measured the differential cross section on argon of charged current ν_e interactions without final-state pions. This paper presents the first single-differential[2] electron-neutrino and antineutrino cross section on argon as a function of the electron energy and scattering angle over the full range. This analysis achieves a final selection efficiency of 21% and a final purity of 72%. The final selected sample contains 243 $\nu_e + \bar{\nu}_e$ candidates in the data. We report the differential cross section as a function of the true kinematic variables using the Wiener single value decomposition (Wiener-SVD) unfolding technique [12][3]. Figure 2 illustrates the unfolded differential cross section as a function of the electron energy and

[1] The fiducial volume is defined as the internal volume excluding 20 cm uniformly from all sides of the TPC

[2] Differential cross sections provide additional kinematic information, and therefore are preferred in the context of performing more precise measurements of the neutrino oscillation parameters.

[3] Data unfolding estimates the actual cross-section value from measurements influenced by the detector response. As a result, unfolded measurements are useful for comparing results across experiments with varying detector responses

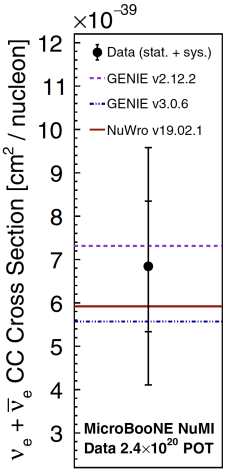

Figure 1: Flux-averaged inclusive electron-neutrino and antineutrino charged-current total cross section. The data cross section (black dot) agrees with the generators GENIE v2.12.2 (purple), GENIE v3.0.6 (blue), and NuWro v19.02.1 (brown) within uncertainties. The inner uncertainty represents statistics only, and the outer represents the total statistics and systematics.

angle. The measurement agrees within uncertainties with four different generators: GENIE v3.0.6 (μB tune), GENIE v3.0.6, NuWro v19.02.2, and GiBUU 2019.

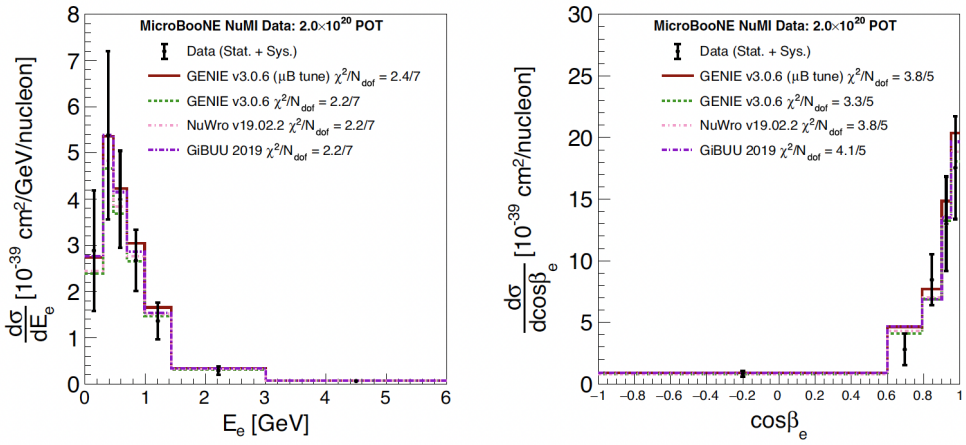

Figure 2: Unfolded differential cross section as a function of the electron (left) energy and (right) scattering angle. The data cross section (black dots) agrees with four different generators: GENIE v3.0.6 (μB tune) (red), GENIE v3.0.6 (green), NuWro v19.02.2 (pink), and GiBUU 2019 (purple).

Updated simulated NuMI flux. The NuMI results above used the NuMI flux model based on the Geant v4.9.2 (with PPFX reweighting) prediction, in which an entire row of shielding blocks was missing from the GDML description of the NuMI beamline. MicroBooNE has since updated its flux simulation to account for this geometry mismatch, and incorporate updated hadron production modelling relevant to the energies and interactions occurring within the NuMI beamline. More details can be found in [13]. Our results, however, are in agreement with cross section extractions using FLUGG, that models the full geometry correctly. Additional fake-data studies indicate that our uncertainty model for these results covers any difference due to the updated flux simulation. MicroBooNE is in the process of producing updated ν_e cross section measurements with higher statistics which fully incorporate the new flux simulation.

BNB Result. The final result covered in this document is the differential cross-section mea-

surement of charged-current interactions without final-state pions [10], published in 2022. The differential cross section is presented as a function of four kinematic variables: electron energy, electron angle with respect to the beam, leading proton energy, and leading proton angle with respect to the beam. This is the first measurement to characterise proton production in neutrino interactions across the visibility threshold.

This measurement uses an accumulated 6.86×10^{20} POT from the BNB beam. The cross section is calculated for two topologies: 1eNp0π and 1e0p0π. Both topologies require charged-current electron-neutrino interactions, with an outgoing electron with kinematic energy $\mathrm{KE}_e >$ 30 MeV, no charged pions with kinematic energy $\mathrm{KE}_\pi > 40$ MeV or any neutral pions. Additional requirements are considered for each case: 1eNp0π classification also requires a kinematic energy of $\mathrm{KE}_p \geq 50$ MeV for the leading proton to ensure they are above the visibility threshold; and 1e0p0π classification also requires $\mathrm{KE}_p < 50$ MeV or no protons, and two extra phase space restrictions on the electron energy ($\mathrm{E}_e > 0.5$ GeV) and the angle between the neutrino beam and electron directions ($\cos\theta_e > 0.6$). An overall final selection efficiency of 17% (12%), a purity of 69% (65%), and 100 (18) true events are selected for the 1eNp0π (1e0p0π) topology.

Similarly to the second NuMI result discussed in this document, the BNB result is also reported as an unfolded differential cross-section, we extract the cross section using an unfolding procedure based on the D'Agostini method [14] and 111 (14) selected signal candidates on data for 1eNp0π (1e0p0π) topologies. Figure 3 shows the unfolded differential cross-section measurement as a function of true electron variables and true proton variables. The data cross section is compared to a variety of neutrino generators: GENIE v3.0.6 (μB tune), GENIE v3.0.6, GENIE v2.12.2, NuWro 19.02.1 and NEUT v5.4.0. The level of agreement is evaluated in terms of the p-values displayed on the plots, as well as the χ^2 between data and generator distribution, whose values can be found on the supplementary material of Ref. [10].

Data prefers GENIE v3.0.6 and NuWro 19.02.1. Both generators present a smaller overall ν_e prediction. The lowest p-value happens for NEUT v5.4.0 which predicts the largest overall cross section. The discrepancy between data and generator models is largest in leading proton angle, with p-values that range from 1% to 7%, and is most pronounced in the forward direction.

5. Conclusion

We have published three electron-neutrino cross-section results, two using NuMI and one using BNB data. These results are pioneering in several aspects: the first ν_e and $\bar{\nu}_e$ inclusive measurement in a large-scale LArTPC on the surface, the first demonstration of the electron-photon dE/dx separation power of LArTPCs using a fully automated analysis chain, the first single-differential ν_e and $\bar{\nu}_e$ cross section on argon as a function of the electron energy and scattering angle, and the first cross-section measurement to characterise proton production in neutrino interactions across the visibility threshold. Our data cross sections are compared to several neutrino generators, such as GENIE v3.0.6 (with and without μB tune), GENIE v2.12.2, NuWro 19.02.1, NEUT v5.4.0, and GiBUU 2019. The two NuMI results [8, 9] agree within uncertainties with all neutrino generators used for each analysis. They do not seem to be sensitive to the difference due to the updated NuMI flux simulation [13]. MicroBooNE is in the processes of producing updated ν_e cross-section measurements with higher statistics which fully incorporate the new flux simulation. The BNB

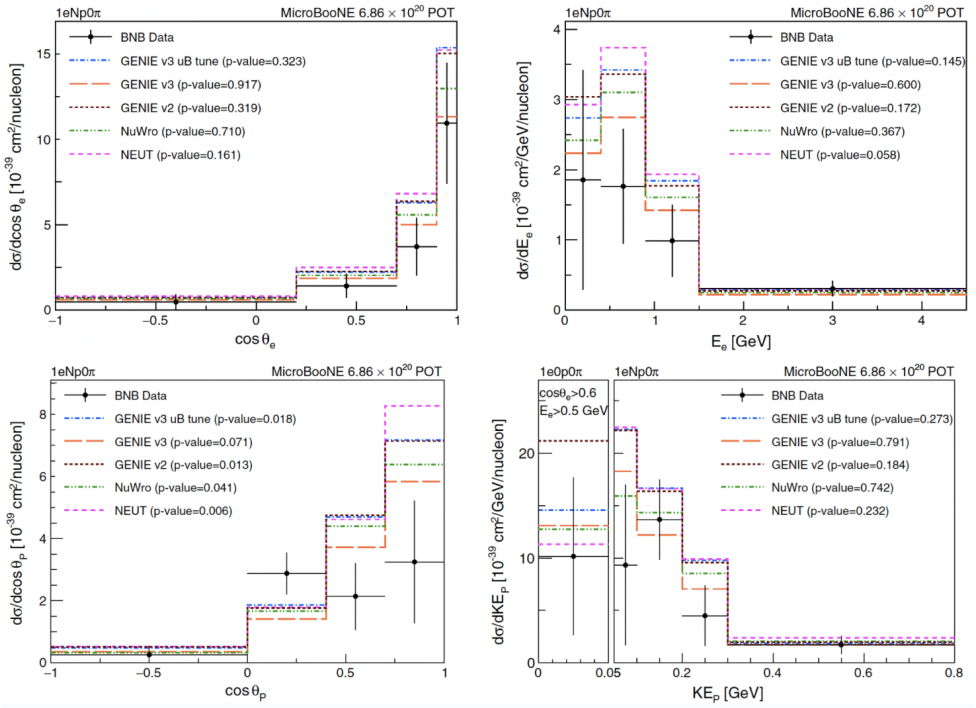

Figure 3: Unfolded cross section as a function of the electron angle with respect to the beam (top left) and electron energy (top right), the leading proton angle with respect to the beam (bottom left) and leading proton energy (bottom right).

result [10] presents a larger discrepancy with the neutrino generators, in particular in the forward direction of the leading proton angle.

References

[1] NOvA Collaboration. Phys. Rev. Lett. **130** 051802 (2023).
[2] T2K Collaboration. Phys. Rev. Lett. **113** 241803 (2014).
[3] T2K Collaboration. Phys. Rev. D **91** 112010 (2015).
[4] T2K Collaboration. J. High Energy Phys. 2020, 114 (2020).
[5] MINERvA Collaboration. Phys. Rev. Lett. **116** 081802 (2016)
[6] Gargamelle Collaboration. Nuclear Physics B 133, 205-219 (1978)
[7] ArgoNeuT Collaboration. Phys. Rev. D **102** 011101 (2020).
[8] MicroBooNE Collaboration. Phys. Rev. D **104** 052002 (2021).
[9] MicroBooNE Collaboration. Phys. Rev. D. **105** L051102 (2022).
[10] MicroBooNE Collaboration. Phys. Rev. D. **106** L051102 (2022).
[11] MicroBooNE Collaboration. Eur. Phys. J. C **78**, 82 (2018).
[12] W. Tang, X. Li, X. Qian, H. Wei, and C. Zhang. J. Instrum. **12**, P1002 (2017).
[13] MicroBooNE Collaboration, MicroBooNE-NOTE-1129-PUB (2024)
[14] G. D'Agostini. arXiv:1010.0632 (2010)